Extreme-ultraviolet polarimeter utilizing laser-generated high-order harmonics

Nicole Brimhall, Matthew Turner, Nicholas Herrick, David D. Allred, R. Steven Turley, Michael Ware, and Justin Peatross

Citation: Review of Scientific Instruments **79**, 103108 (2008); doi: 10.1063/1.2999543
View online: http://dx.doi.org/10.1063/1.2999543
View Table of Contents: http://scitation.aip.org/content/aip/journal/rsi/79/10?ver=pdfcov
Published by the AIP Publishing

Extreme-ultraviolet polarimeter utilizing laser-generated high-order harmonics

Nicole Brimhall, Matthew Turner, Nicholas Herrick, David D. Allred, R. Steven Turley, Michael Ware, and Justin Peatross[a)]
Department of Physics and Astronomy, Brigham Young University, Provo, Utah 84602, USA

(Received 24 March 2008; accepted 17 September 2008; published online 27 October 2008)

We describe an extreme-ultraviolet (EUV) polarimeter that employs laser-generated high-order harmonics as the light source. The polarimeter is designed to characterize materials and thin films for use with EUV light. Laser high harmonics are highly directional with easily rotatable linear polarization, not typically available with other EUV sources. The harmonics have good wavelength coverage, potentially spanning the entire EUV from a few to a hundred nanometers. Our instrument is configured to measure reflectances from 14 to 30 nm and has ~180 spectral resolution ($\lambda/\Delta\lambda$). The reflection from a sample surface can be measured over a continuous range of incident angles (5°–75°). A secondary 14 cm gas cell attenuates the harmonics in a controlled way to keep signals within the linear dynamic range of the detector, comprised of a microchannel plate coupled to a phosphorous screen and charge coupled device camera. The harmonics are produced using ~10 mJ, ~35 fs, and ~800 nm laser pulses with a repetition rate of 10 Hz. Per-shot energy monitoring of the laser discriminates against fluctuations. The polarimeter reflectance data agree well with data obtained at the Advanced Light Source Synchrotron (Beamline 6.3.2). © *2008 American Institute of Physics.* [DOI: 10.1063/1.2999543]

I. INTRODUCTION

The extreme-ultraviolet (EUV) wavelength range [i.e., ~1–~100 nm or ~10–~1000 eV) is important to photolithography, space-based astronomy, and microscopy.[1–3] Virtually all materials that might be used for optical elements are highly absorptive in most of this wavelength range. Thus, transmissive optics are for the most part precluded, and reflective optics typically require multilayer coatings to reach feasible reflectivities. To design such multilayers, the indices of refraction of coating materials need to be well characterized. Unfortunately, the optical properties of many materials in this wavelength range are unknown or not completely characterized.[4–6]

Laser-generated high harmonics provide an excellent source of polarized, directional EUV light that can be used to characterize materials. We have developed an EUV polarimeter based on the high harmonics, which form a frequency comb throughout the EUV. Our setup utilizes harmonics of an 800 nm Ti:sapphire laser. Here we present measurements made using harmonic wavelengths from 14 to 30 nm; however, the instrument could conceivably operate through other ranges of harmonic wavelengths. An advantage of high harmonics is their preservation of the generating laser's linear polarization.[7] This allows the polarization of high harmonic EUV light to be easily rotated using a half-wave plate in the generating laser beam. This feature is challenging to duplicate with unpolarized sources such as plasmas because of the difficulty in producing efficient and broadband polarizing optics in the EUV. Synchrotron light is naturally polarized but the polarization is not easily rotated. While the sample and detection system can be rotated axially around a synchrotron's EUV beam, this approach is technically challenging and not available at all synchrotron sources [e.g., at the Advanced Light Source (ALS)]. The instrument described in this article can make polarization-resolved reflectance measurements at multiple incident angles. Separate measurements of *s*- and *p*-polarized reflectivities generate effectively two distinct sets of data, rather than one set, as is the case for unpolarized or fixed-polarization sources.

Another advantage of the laser harmonic source is its compact footprint and affordability when compared to synchrotron sources. These features make it a feasible "in-house" instrument at facilities developing EUV thin films, enabling rapid turn-around time for film characterization, and increasing the opportunities for making *in situ* measurements during the thin-film deposition process. While the brightness and wavelength coverage of the high harmonic source are less than those of a synchrotron source, they are sufficient for these types of measurements.

Our instrument, shown schematically in Fig. 1, measures the reflectance from a sample surface as a function of incident angle, light polarization orientation, and wavelength. The instrument can be used to characterize EUV properties of materials and to quantify the performance of multilayer coatings designed for the EUV. Measurements obtained with the polarimeter described here agree well with measurements taken at the ALS[8] in Berkeley, California (Beamline 6.3.2).

II. HIGH HARMONIC EUV LIGHT SOURCE

The high harmonics used by the polarimeter are generated with 800 nm, 35 fs, and ~10 mJ laser pulses focused in a cell of helium, neon, or argon gas. The laser pulses are focused using $f/125$ optics to approximately 10^{15} W/cm^2

[a)]Electronic mail: peat@byu.edu.

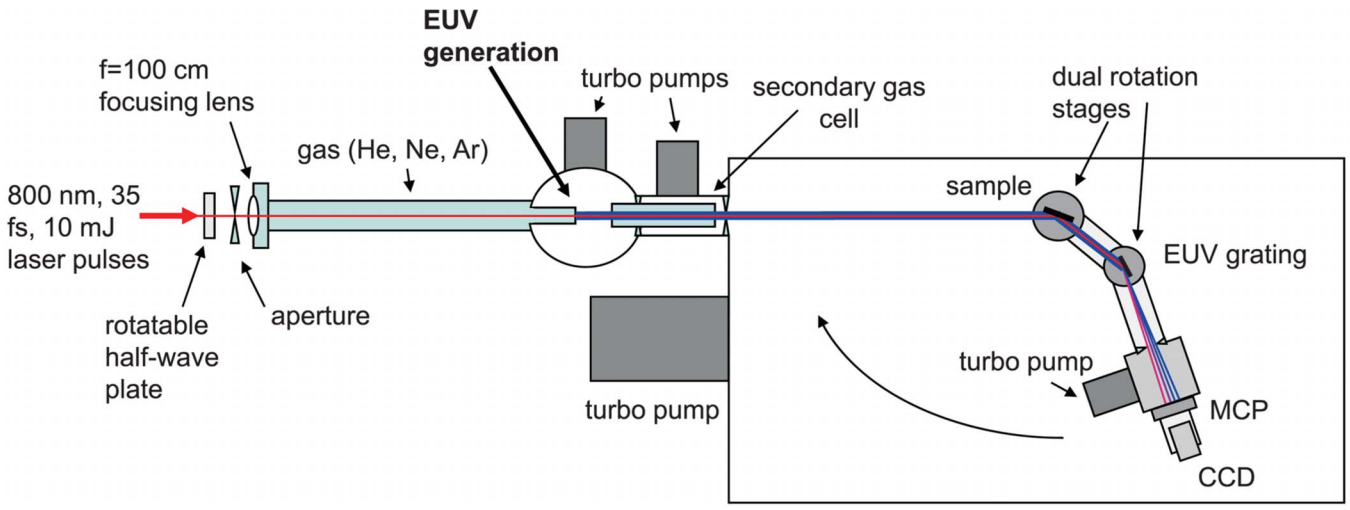

FIG. 1. (Color online) Polarimeter schematic (top view). 800 nm, 35 fs, and 10 mJ laser pulses are focused into a cell of helium, neon, or argon gas to generate harmonics. A half-wave plate in the generating laser rotates the linear polarization of the laser and harmonics. Harmonics emerge from the focus in a narrow beam, which travels through the secondary gas cell to the sample. Reflected harmonics are separated and focused with a grating and imaged onto a MCP.

inside the gas.[9–11] A wide comb of odd harmonic frequencies (with wavelengths distributed throughout the EUV) emerges from the focus in a narrow beam, embedded in the residual laser beam. The harmonics take on the same polarization as the linearly polarized generating laser. In our setup, the high harmonics are typically produced in 100 torr of helium gas (harmonic orders 39–73), 57 torr of neon gas (orders 27–57), or 12 torr of argon gas (orders 15–31). An aperture is placed immediately before the focusing lens at an optimal diameter of 1.1 cm, and the molybdenum exit foil that caps the gas cell is positioned 100 cm from the focusing lens. The harmonics are produced in the final ~1 cm of gas before the foil, and the laser and harmonics exit the cell via a hole drilled by the laser through the foil.

High harmonics are detected using a grazing-incidence tungsten-coated grating (1200 lines/mm, 2° blaze, 2 m radius of curvature or 600 lines/mm, 2° blaze, 1 m radius of curvature), which separates the different harmonic orders and focuses them onto a microchannel plate (MCP) coupled to a phosphor screen. Each harmonic order strikes the detector at a different horizontal position, while the angular spread of each harmonic beam is preserved in the vertical dimension. An example spectrum seen at our detector is shown in Fig. 2, where the harmonic spectrum extends about 15 mm on the active area of the MCP.

The wavelength of an individual harmonic is λ_0/q, where λ_0 is the wavelength of the generating laser (λ_0 =800 nm) and q is the harmonic order (an odd integer). Other groups demonstrated the generation of up to several hundred harmonic orders[12–14] (although with less flux) using different gas-laser interaction geometries and shorter pulse durations than we have used.

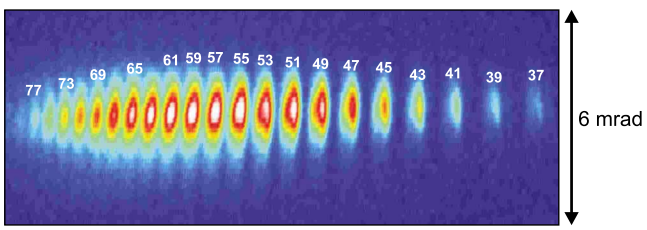

FIG. 2. (Color online) Harmonics of orders 37–77 (wavelengths 10.4–21.6 nm) produced in helium gas. Each harmonic order strikes the detector at a different horizontal position on the MCP detector, while the angular width of each harmonic beam is preserved in the vertical dimension.

The wavelength range of harmonics seen in Fig. 2 is 10–20 nm. Although the spectrum is not continuous like a synchrotron source, the harmonics have good wavelength coverage throughout the range. The highest-order harmonics merge together, giving quasicontinuous wavelength coverage in some ranges. With our 10 Hz laser system, the flux of energy in a given order of the high harmonics is approximately 6×10^8 photons/s.[9] The finite size of the harmonic generating region (~100 μm across) effectively functions as an input slit for the instrument, resulting in a spectral resolution of about 180 for our grazing-incidence spectrometer. This resolution is not as good as available at the ALS with its higher flux ($\lambda/\Delta\lambda\approx7000$), but it is sufficient to resolve many spectral features of optical samples. Spectral resolution is considered further in Sec. III D.

III. POLARIMETER DESIGN

On the measurement side of the polarimeter, the primary optical elements are the sample surface, the grating, and the MCP detector (Burle APD 3025FM 12/10/12 I CSI P20), which has an active area about 25 mm wide. In Secs. III A and III B we discuss the automated positioning system used to align these elements. Sections III C and III D cover how the wavelength of each harmonic and the spectral resolution of the instrument were determined. In Sec. III E we discuss the secondary gas cell shown in Fig. 1, which introduces controlled beam attenuation to avoid detector saturation when the signal is strong. Finally, in Sec. III F we show how the effects of power fluctuations in the harmonic signal were mitigated.

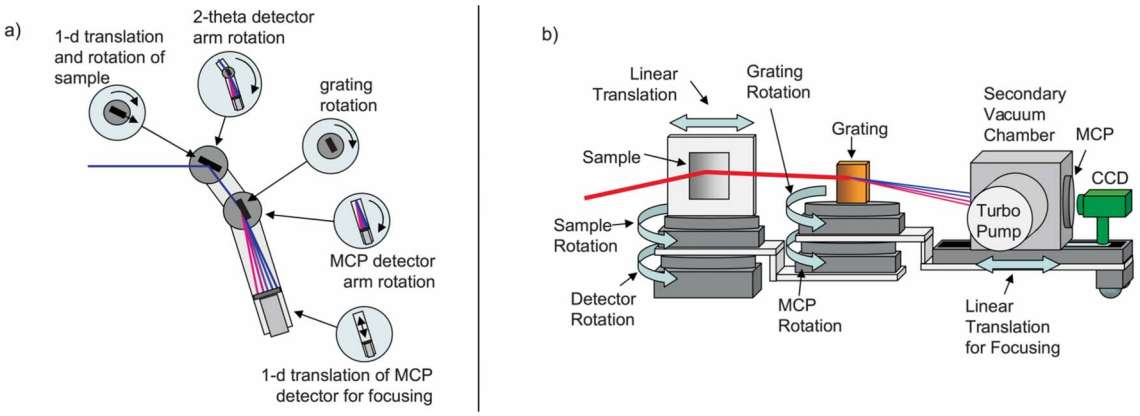

FIG. 3. (Color online) Polarimeter positioning system (a) top view and (b) side view. Incident harmonics are reflected from a sample that can be rotated to measure reflectance as a function of angle. A second rotation stage beneath the sample rotates the entire detection system through twice the sample angle. The EUV grating can also be rotated to measure different wavelength ranges of harmonics. A second rotation stage under the grating rotates the detector.

A. Positioning system

The positioning system is made up of four rotation stages and two linear translation stages controlled by a single computer, as illustrated in Fig. 3. The sample or test surface is mounted above two concentric rotation stages (ThorLabs NanoRotator NR360S). One stage varies the incident angle of the harmonic light on the sample. This provides measurements of sample reflectance as a function of incident angle. The other stage swings the entire detection system (grating and MCP detector) through twice that angle, allowing detection of reflected light. A second pair of rotation stages sits beneath the grating at a distance of 15 cm from the sample. One of these rotation stages adjusts the grating angle, and the other separately adjusts the angle of the MCP to allow detection of diffracted light. A linear translation stage is used beneath the MCP detector to focus the harmonic orders of interest onto the detector. A typical grating angle is 4°, and a typical distance from the grating to the MCP is 30 cm. The sample holder is also connected to a linear translation stage. This allows the sample to be moved out of the beam to obtain incident-intensity measurements of harmonics.

The diffraction grating is placed after the sample, which allows simultaneous reflectance measurements of a range of wavelengths. The different harmonic orders are spatially separated on the MCP and recorded with a charge coupled device (CCD) camera. We can measure the reflectance for 10–20 consecutive odd harmonic orders simultaneously.

The polarimeter positioning system is housed in a vacuum chamber with approximate dimensions 1.5×1 m^2, which is evacuated to about 10^{-4} torr. The MCP detector must be operated at pressures lower than 10^{-5} torr so we placed a small vacuum chamber (Lesker CU6–0450) inside the large vacuum chamber. This secondary vacuum chamber has its own turbo pump and a 5 mm aperture for the harmonics to enter. With differential pumping, this secondary chamber can reach base pressures lower than 10^{-6} torr. The entire system can pump to the necessary pressures in under 30 min from startup.

B. Alignment diagnostic

The secondary vacuum chamber (15 kg) and the turbo pump (3 kg) are major contributors to weight on the long (~45 cm) rotating arm. We use ball-bearing wheels under the secondary vacuum chamber to carry the weight of the assembly. However, owing to the weight of the positioning stages and the secondary vacuum chamber, the torque limit of 23 N cm is seriously exceeded on two of the rotation stages. As a result, the positioning error compounds to as poor as 1°, which is clearly unacceptable. For example, to repeatedly position a given harmonic order within 1 mm on the detector, the first rotation stage must have positioning accuracy of 0.1°, and the second 0.2°. (Recall that the sample to grating distance is approximately 15 cm while grating to MCP distance is approximately 30 cm).

To address this issue, we implemented an alignment diagnostic that employs a tightly collimated HeNe 633 nm laser. The laser enters the large vacuum chamber through a lens in a side port. A solenoid toggles a temporary mirror into position at any time during a measurement run, allowing the HeNe laser to propagate along the same path as the harmonics into the spectrometer. The HeNe laser has a <1 mm spot size on the diffraction grating. A CCD camera views the HeNe laser spot on the diffraction grating surface. A second CCD positioned inside the secondary vacuum chamber observes where the zero-order reflection from the grating strikes the MCP surface.

After initial positioning of the rotation stages, fine adjustments can be made first to center the HeNe laser on the diffraction grating and second to cause the HeNe beam to strike a predetermined location on the interior of the MCP. This procedure allows the first stage to be set with a positioning accuracy better than 0.1° and the second stage to better than 0.2°. We found that the positioning system was accurate enough for us to easily distinguish harmonic orders from each other. Because of the sharpness of some of the harmonic peaks, we are able to align the harmonic spectral images further using software, making the effective angle positioning accurate to about 0.01°. Using both of these techniques, we are able to obtain a spectral resolution ($\lambda/\Delta\lambda$) of 180 (discussed in Sec. III D).

C. Determination of orders

To determine the wavelength of each harmonic, we placed a 0.2 μm aluminum filter on a solenoid so that it

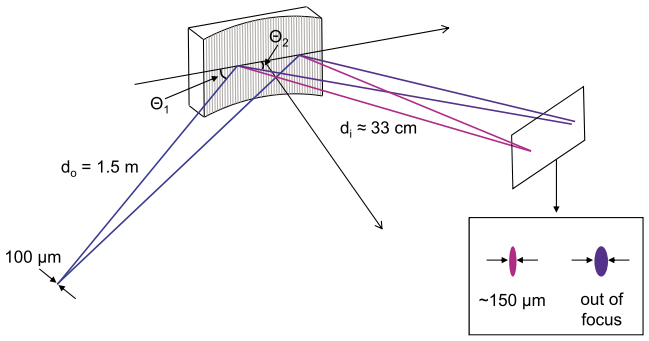

FIG. 4. (Color online) Schematic of setup for ray-tracing program to determine spectral resolution. Representative rays are traced from a 100 μm extended light source to the grating, situated 1.5 m away and oriented 4° from grazing and then to the MCP surface an additional 30 cm afterward.

could be moved into and out of the harmonic beam before the sample while under vacuum. The aluminum $L_{2,3}$ edge transmits harmonics of order 47 and below, but not harmonic orders 49 and above. By moving the filter into the beam while observing harmonics, we can quickly identify the 47th order. From there we simply count orders to calibrate the rest of the harmonic spectrum.

D. Spectral resolution

The harmonic source itself serves effectively as the entrance slit of the polarimeter/spectrometer. We developed a simple ray-tracing program to characterize the defocusing of the harmonics at the detector due to the finite size of the source and aberrations from the geometry of the spherical grating surface. We traced representative rays from a 100 μm extended light source to the grating situated 1.5 m away oriented 4° from grazing, and then to the MCP surface an additional 30 cm afterward (see Fig. 4). The location of the focusing (or image distance) is given by

$$\frac{\sin^2\theta_1}{d_o} + \frac{\sin^2\theta_2}{d_i} = \frac{\sin\theta_1 + \sin\theta_2}{r}, \quad (1)$$

where θ_1 is the incident angle of the light on the grating measured from grazing, θ_2 is the diffracted angle of the light measured from grazing, d_o is the object distance, d_i is the image distance, and r is the radius of curvature of the focusing diffraction grating.[15,16]

For typical harmonic beams with 3 mrad divergence arising from a 100 μm source, the maximum spread at the detector is 150 μm (rather than an ideal line), whereas the typical separation between harmonic lines is approximately 1 mm. The finite width of harmonic lines is partly due to the fact that we observe multiple wavelengths on a single plane, whereas different harmonics focus best with different grating-MCP spacings. Since harmonic features can be lined up effectively to within 30 μm using software, aberrations in the grating imaging system are the limiting factor in the spectral resolution.

As can be seen in Fig. 5, harmonic peaks appear to sit on top of a quasicontinuous spectrum. The previous analysis suggests that the apparent continuous spectrum does not arise merely from aberrations in the imaging system, and the sharpness of the harmonic peaks within the image provide

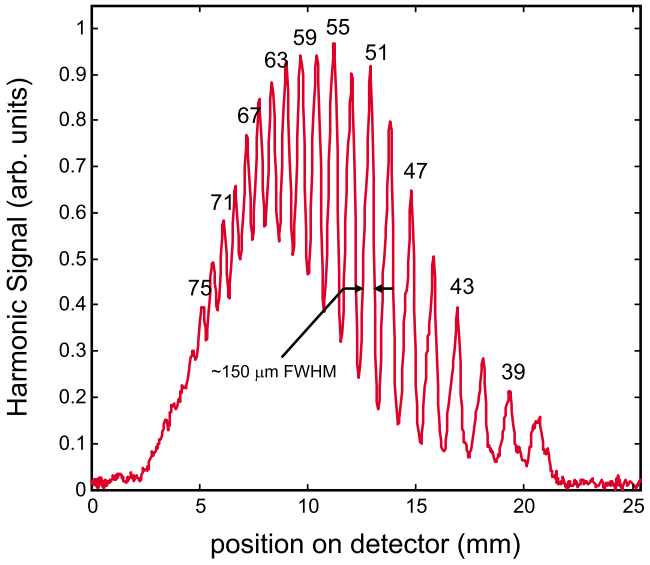

FIG. 5. (Color online) Harmonic signal as a function of position on the MCP detector. Harmonics orders from 37 to 77 were generated in helium gas.

direct evidence of good spectral resolution. There may be multiple regimes of harmonic-generation within the generating volume, some regions giving rise to sharp orders, and others contributing shifted or broadened peaks of EUV wavelengths due to chirping of the generating pulse[17] or self-steepening of the leading edge of the pulse.[11] The harmonics from these various regions can merge together to give broader spectral coverage.

As indicated in Fig. 5, the 43rd and 63rd harmonics are separated by 8.6 mm on the detector. This represents a change of 5.9 nm in wavelength. The blurring of the peaks by 150 μm corresponds to a change in wavelength of 0.10 nm, which corresponds to a spectral resolution of about 180 for the 43rd harmonic ($\lambda = 18.6$ nm).

E. Controlled harmonic attenuation

In the EUV, most materials are not highly reflecting except near grazing incidence. For this reason, a measurement of reflectance as a function of grazing-incidence angle made through a significant range of angles can span three or four orders of magnitude. Our MCP/camera system does not have sufficient dynamic range to span this variation. We increase the dynamic range of our detection system with a secondary gas cell that acts as a controlled harmonic attenuator. The secondary gas cell is 14 cm long, and is placed in the path of the laser after harmonics are generated, far enough downstream so that the laser cannot ionize the gas or generate additional harmonics. Neon gas can be added to the cell (usually between 0 and 3 torr measured with a manometer), which attenuates harmonics up to three orders of magnitude. At grazing incidence where signal is high, gas is added to decrease the signal, while at near-normal angles, no gas is added. Thus high and low signal can be measured with similar exposure to the detector. The actual signal level is later obtained using the absorption coefficient of neon, which is well characterized.[18]

F. Laser power discriminator

The stability of our high harmonic source is important to the accuracy of the polarimetry measurements. Reflectance measurements are defined as reflected signal divided by incident signal so drifts in harmonic signal between the two measurements can skew the result. Small variations or drift in pump laser energy or gas pressure near the exit of the generating gas cell can translate into large variations in harmonic output because of the high nonlinearity in the harmonic-generation process. We have observed that shot-to-shot variations in our laser-pulse energy lead to large variation in harmonic signal. This variability can be mitigated to some degree by averaging 100 shots (10 s) for each data point.

To further improve repeatability, we implemented a laser-pulse energy discriminator. An optical fiber transmits a small sample of the incident laser beam to an unused corner on the outside surface of the MCP detector. The light from the fiber is thus captured in the same image that records the harmonic spectra, providing real-time monitoring of the laser power. A computer selects only shots where the incident laser energy falls within a user-specified range and averages 100 "acceptable" harmonic images. By decreasing the range of acceptable laser energy, the repeatability of the measurements improves markedly. For our system, a 10% laser-energy window selects about one image out of three and reduces the variability in harmonic signal significantly. However, laser-power variation is not the only systematic error we have in our system. For example, changes in the spatial profile of the gas in the region of harmonic generation (as happens when the laser continues to drill through the exit foil during a scan) can cause error in our measurements.

IV. REFLECTANCE MEASUREMENTS

To benchmark the performance of our instrument, we used a silicon substrate with a thermally oxidized layer as a test sample. Spectroscopic ellipsometry using visible light showed the sample to have an oxide layer thickness of 27.4 nm $\pm$ 0.2 nm. This thickness causes interferences between the front and back surfaces of the silicon dioxide layer. Thus, "fringes" are seen as the angle of incidence is varied. These fringes provide features to compare with data taken using other sources and with computed data. Silicon dioxide over silicon also has the advantages of being stable in air for long periods of time, and the two surfaces of the oxide can be exceptionally uniform and smooth. However, we found that it was difficult to keep samples free of contaminants such as hydrocarbons that diminish reflectance over time. To minimize the contamination problem for this test, we made measurements within a couple of hours of cleaning our sample with a xenon excimer lamp (Resonance LTD). In future work, we will explore adding an *in situ* plasma cleaner (Evactron), which has significantly reduced the accumulation of hydrocarbons in other experimental chambers that we have used.

All measurements were averaged over 100 shots and the accepted variation in the laser power was $\pm 5\%$. The reflected light intensity signal was determined by first averaging the CCD data in the vertical dimension over the area containing harmonic signal. Harmonic order was determined using the method discussed in Sec. III C. The reflected signal for each harmonic order was taken to be the local maximum in the line-out data. The dark signal was determined by averaging over a region of the MCP away from the harmonics. The dark signal was subtracted from the region of harmonic signal.

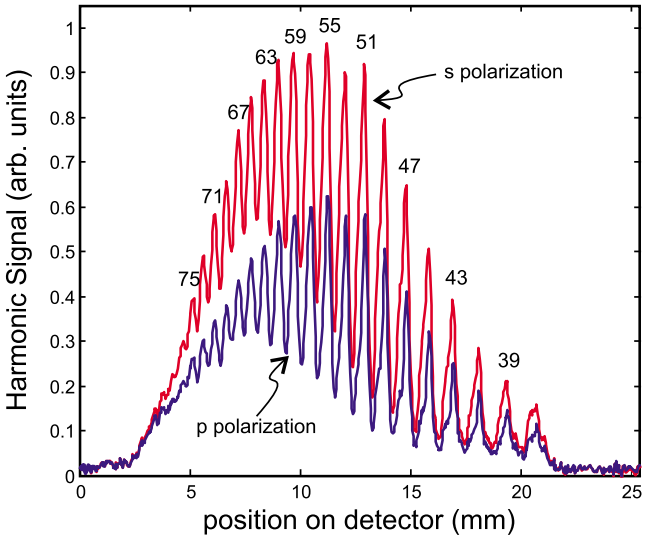

FIG. 6. (Color online) *s*- and *p*-polarized harmonics reflect differently from the EUV grating. Accordingly, each reflectance measurement was normalized using the incident measurement of the same polarization.

The secondary gas cell was used to attenuate the signal as necessary to avoid detector saturation, in particular, when measuring the incident beam or the reflected beam near grazing incidence. Pressures in the secondary cell ranged in value from 0 to 2.8 torr. The attenuation coefficient of neon[18] was then used to correct the signal. The incident harmonic signal (before the sample) was measured three different times during the run, at the beginning, middle, and end, to guard against possible drift in harmonic flux during the experiment. The variations between these measurements were on the order of the uncertainty in a given measurement.

As would be expected, *s*- and *p*-polarizations were found to reflect from the EUV grating somewhat differently (see Fig. 6), so each reflectance measurement was normalized using the incident measurement of the same polarization. The reflectance R from the sample was computed for either *s*- or *p*-polarized light as

$$R = (R_{\mathrm{sig}} - D)/(I - D), \tag{2}$$

where R_{sig} is the reflected light intensity signal, D is the dark signal, and I is the incident light intensity signal. Reflectance for *s*- and *p*-polarized lights is shown in Fig. 7 for representative wavelengths of 14.0, 15.7, 20.5, and 29.6 nm. The ability to make separate *s*- and *p*-polarized reflectance measurements in this wavelength range is a strong advantage of this instrument. Also plotted for comparison are *s*- and *p*-polarized reflectances computed from the optical constants of SiO_2.[18] The measured data match the computed data reasonably well. Especially important, measured data match the locations of interference fringes in the computed data. The

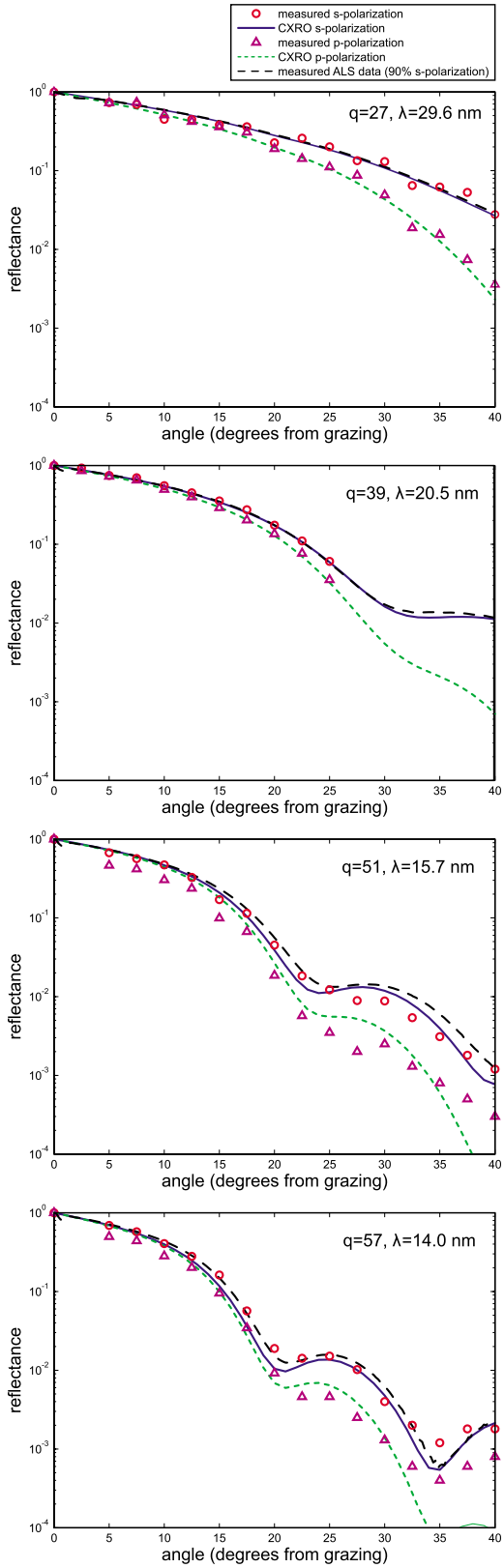

FIG. 7. (Color online) Measured *s*- and *p*-polarized reflectance (circles and triangles) from a silica sample. Also plotted are *s*- and *p*-polarized reflectance computed using the optical constants of SiO_2 (solid and small-dashed lines)[18] and reflectance data measured at Beamline 6.3.2 of the ALS (90% *s*-polarized, long-dash line).

poorest agreement in measured and computed data is when signal is very low. At low signal, we encounter a measurement "floor" at a reflectance of about 5×10^{-4}. This might be improved in the future by increasing the brightness of our incident harmonics. We also made reflectance measurements from the same sample at Beamline 6.3.2 of the ALS at Lawrence Berkeley National Laboratories for comparison. EUV light from Beamline 6.3.2 is polarized at 90% *s*- and 10% *p*-polarizations by intensity.

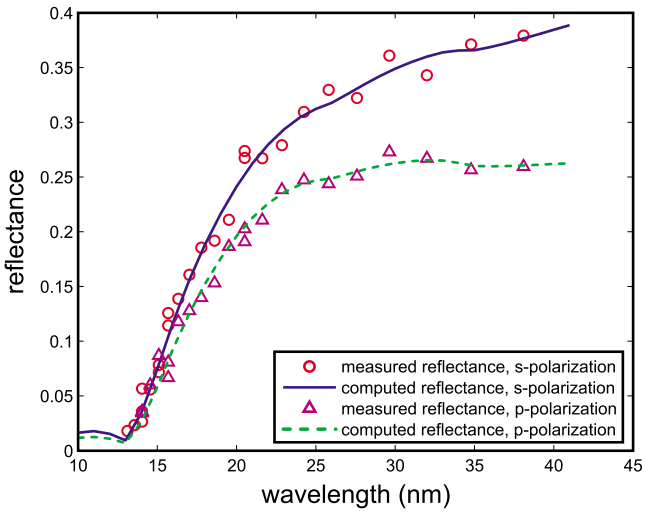

FIG. 8. (Color online) Measured *s*- and *p*-polarized reflectances (circles and triangles) from a silica sample as a function of wavelength at an incident angle of 17.5° from grazing. Also plotted are *s*- and *p*-polarized reflectances computed using the optical constants of SiO_2 (solid and dashed lines).[18]

Figure 8 depicts reflectance as a function of wavelength at a sample angle of 17.5° from grazing measured with the polarimeter and computed using the optical constants of SiO_2.

V. CONCLUSIONS

We have developed and characterized an instrument that utilizes polarized laser-generated EUV light to measure reflectance from thin-film samples as a function of angle. The laser high harmonics are shown to have sufficient flux for reflection measurements with a wide wavelength range and easily rotatable linear polarization. This "workhorse" application of high harmonics can facilitate our understanding of EUV materials and optics employed in varied applications. Our instrument incorporates a versatile positioning system and can resolve spectral features with a resolution of about 180. We have implemented a secondary gas cell for use as a controlled harmonic attenuator for increased dynamic range in our MCP-based detector system. The reflectance data taken with the polarimeter agree well with data taken from the same sample at Beamline 6.3.2 at the ALS and with data computed using the optical constants of SiO_2.

ACKNOWLEDGMENTS

We acknowledge Elise Martin, Joseph Muhlestein, and Elizabeth Strein, as well as support staff at the Advanced Light Source for assistance with measurements. This work was supported by the National Science Foundation under Grant No. PHY-0457316.

[1] B. R. Sandel, A. L. Broadfoot, C. C. Curtis, R. A. King, T. C. Stone, R. H. Hill, J. Chen, O. H. W. Siegmund, R. Raffanti, D. D. Allred, R. S. Turley, and D. L. Gallagher, Space Sci. Rev. **91**, 197 (2000).
[2] G. L. T. Chiu and J. M. Shaw, http://www.research.ibm.com/journal/rd/411/chiu.html, accessed 21 January 2008.
[3] A. Hirai, K. Takemoto, K. Nishino, B. Niemann, M. Hettwer, D. Rudolph, E. Anderson, D. Attwood, D. P. Kern, Y. Nakayama, and H. Kihara, Jpn. J. Appl. Phys., Part 1 **38**, 274 (1999).
[4] B. Sae-Lao and R. Soufli, Appl. Opt. **41**, 7309 (2002).
[5] R. Soufli and E. Gullikson, Appl. Opt. **37**, 1713 (1998).
[6] M. Fernández-Perea, J. I. Larruquert, J. Aznarez, J. Mendez, M. Vidal-Dasilva, E. Gullikson, A. Aquila, R. Soufli, and J. L. G. Fierro, J. Opt. Soc. Am. A **24**, 3800 (2007).
[7] D. Schulze, M. Dorr, G. Sommerer, J. Ludwig, P. Nickles, T. Schlegel, W. Sandner, M. Drescher, U. Kleineberg, and U. Heinzmann, Phys. Rev. A **57**, 3003 (1998).
[8] E. Gullikson, S. Mrowka, and B. Kaufmann, Proc. SPIE **4343**, 363 (2001).
[9] J. C. Painter, M. Adams, N. Brimhall, E. Christensen, G. Giraud, N. Powers, M. Turner, M. Ware, and J. Peatross, Opt. Lett. **31**, 3471 (2006).
[10] N. Brimhall, J. C. Painter, N. Powers, G. Giraud, M. Turner, M. Ware, and J. Peatross, Opt. Express **15**, 1684 (2007).
[11] M. Turner, N. Brimhall, M. Ware, and J. Peatross, Opt. Express **16**, 1571 (2008).
[12] A. L'Huillier and P. Balcou, Phys. Rev. Lett. **70**, 774 (1993).
[13] A. Rundquist, C. G. Durfee III, Z. Chang, C. Herne, S. Backus, M. M. Murnane, and H. Kapteyn, Science **280**, 1412 (1998).
[14] E. Takahashi, Y. Nabekawa, T. Otsuka, M. Obara, and K. Midorikawa, Phys. Rev. A **66**, 021802 (2002).
[15] A. Thompson, D. Attwood, E. Gullikson, M. Howells, K. J. Kim, J. Kirz, J. Kortright, I. Lindau, P. Pianetta, A. Robinson, J. Scofield, J. Underwood, D. Vaughan, G. Williams, and H. Winick, *X-Ray Data Booklet* (Lawrence Berkeley National Laboratory, University of California, Berkeley, CA, 2001).
[16] H. Noda, T. Namioka, and M. Seya, J. Opt. Soc. Am. **64**, 1031 (1974).
[17] T. Sekikawa, T. Kumazaki, Y. Kobayashi, Y. Nabekawa, and S. Watanabe, J. Opt. Soc. Am. B **15**, 1406 (1998).
[18] B. L. Henke, E. M. Gullikson, and J. C. Davis, At. Data Nucl. Data Tables **54**, 181 (1993).